Received: 1 February 2023 | Revised: 16 August 2023 | Accepted: 17 August 2023

DOI: 10.1002/hyp.14979

RESEARCH ARTICLE

WILEY

From cave to spring: Understanding transport of suspended sediment particles in a fully phreatic karst conduit using particle analysis and geochemical methods

Yanina K. Mueller[1] | Nico Goldscheider[1] | Elisabeth Eiche[2] | Hanna Emberger[1] | Nadine Goeppert[1]

[1]Karlsruhe Institute of Technology (KIT), Institute of Applied Geoscience, Chair of Hydrogeology, Karlsruhe, Germany

[2]Karlsruhe Institute of Technology (KIT), Institute of Applied Geoscience, Chair of Geochemistry & Economic Geology, Karlsruhe, Germany

Correspondence
Yanina K. Mueller, Karlsruhe Institute of Technology, Adenauerring 20b, Karlsruhe 76131, Germany.
Email: yanina.mueller@kit.edu

Funding information
Deutsche Forschungsgemeinschaft; Publication Fund of the Karlsruhe Institute of Technology

Abstract

Karst aquifers are vulnerable to contamination, especially in the context of heavy rainfall events. Contamination is often associated with turbidity that can originate from the soil zone, infiltrating surface waters or resuspension of previously deposited sediments within the aquifer. While turbidity events can be well monitored at karst springs, related information about the sediment origin and the spatiotemporal input function usually remain unknown. Thus, the mobility and attenuation of the particulate matter and associated pollutants can hardly be determined quantitatively. A tracer test with suspended cave sediments and solute tracers for comparison has hence been performed in a karst aquifer at the Blue Spring (Blautopf) in Southern Germany. The tracers were injected in the cave system, at the beginning of a fully phreatic karst conduit, and monitored at the spring after a travel distance of 1250 m. The particle-size distribution was monitored using a particle counter and sediment samples were filtered with 0.45-µm cellulose acetate filters. Particles on the filter were analysed for major and trace elements as well as rare earth elements (REE) by ICP-MS after acid digestion. Results show that (1) sediment particles were transported faster than solutes, which was interpreted as a transport in the main flow path of the conduit, whereas conservative tracers tend to diffuse into smaller fissures as well. (2) All measured particles sizes were transported at similar flow velocities. (3) A transport associated to sediment particles could be shown for all measured elements. This study presents a methodological improvement of comparative sediment tracer tests as well as deeper insights into particle and element transport processes in karst aquifers, originating from previously deposited cave sediment. Results provide deeper knowledge into transport processes of sediment-associated contaminants, such as heavy metals which may strongly be affected by the particle size. This knowledge contributes to a better management of karst water resources in the context of turbidity events.

This is the first study that investigates the transport of geochemical elements associated with sediment particles in a karst conduit system by means of comparative tracer tests. This is relevant, because sediments play an important but hitherto poorly understood role in the transport and retention of pollutants in karst aquifers.

KEYWORDS
conservative tracer, contamination, geochemistry, karst, particle transport, sediment

1 | INTRODUCTION

About 9.2% of the world's population withdraw their drinking water from karst aquifers (Stevanović, 2019). Typical properties of karst aquifers are highly variable discharge regimes originating from fast and turbulent flow in open fissures and conduits. Especially in case of heavy rainfall events there is a high degree of particle mobilization, both aquifer-derived and soil-derived, resulting in a high water turbidity (Goldscheider & Drew, 2007; Herman et al., 2008; Pronk et al., 2006; Vuilleumier et al., 2021). Clastic sediment deposits inside the karst system originate both from weathering residues of surrounding rocks as well as sediment and soil that entered the cave system during previous rainfall events or through sinkholes and sinking streams. Typically, cave sediments are a mixture of silt, clay, sand and larger rock fragments (Cholet et al., 2019; Vesper & White, 2004).

Sediment deposits in caves serve as habitat for microbial communities and play a major role for cave ecosystems (Adetutu et al., 2012; Goldscheider et al., 2006; Zhu et al., 2019). Furthermore, organic compounds or heavy metals can be retained and stored in cave sediments and later be remobilized again during flood events (Vesper et al., 2001). In this context, smaller particles have a larger relative surface area and thus tend to have a higher sorption capacity for example for organic substances, trace metals and heavy metals (Atteia & Kozel, 1997; Churchman & Velde, 2019; Horowitz & Elrick, 1987; Huang et al., 2020). Chemical conditions, in particular pH and redox environment, determine the solubility and affinity of metals to bind to mineral surfaces and thus impact the mobility of metals. Redox sensitive elements are for example Mn, Fe, Al, Cr or Ce. The latter for example occurs in the tetravalent form Ce^{4+} under oxidizing conditions and is primarily fixed to particles, such as Fe–Mn (hydr)oxides (Braun et al., 1990; Brioschi et al., 2013; Gwenzi et al., 2018; O'Connor et al., 2015; Stecko & Bendell-Young, 2000). Sediment deposits can act thus as a major sink for natural substances as well as metals of previous contamination events. Suspended sediment particles not only serve as transport vectors for pathogens, such as bacteria, viruses or protozoa, but also for organic contaminants, major and trace elements, including heavy metals and rare earth elements (REE) (Horowitz et al., 2008; Huang et al., 2020; Jung et al., 2014; Mahler et al., 2000).

The concentration of REE in sediments is dependent on the contained minerals and their respective source area, for further information on REE please refer to for example Aide and Nakajima (2020), LaMoreaux (2019) and McLennan (2001). Besides a geogenic origin, REE concentrations in an aquifer can be increased by anthropogenic input. Gadolinium (Gd) is used, for example in medicine, and is merely retained by waste water treatment plants, thus can enter the environment, resulting in an enrichment relative to other REE (Bau & Dulski, 1996; Künnemeyer et al., 2009; Möller et al., 2000).

A possibility to investigate sediment particle transport under near-natural conditions in a karst system is a tracer test with an injection of natural sediments and a conservative solute tracer for comparison. In contrast to natural particle transport in karst systems, which is usually initiated by shear stress, the sediment during a sediment tracer test is injected as a suspension in form of a Dirac input. Previous studies also describe the use of microspheres, which however exhibit different surface properties in contrast to natural silica particles that can lead to lower mass recoveries (Harvey et al., 2008; Schiperski et al., 2016; Sinreich et al., 2009). Several studies describe higher flow velocities of particles in comparison to solutes, which make a detailed understanding of particle transport behaviour in karst aquifers crucial. Pathogens and contaminants can be transported in dissolution, in particulate form (e.g. bacteria) or adsorbed to particles (Vesper et al., 2001). A differing transport behaviour of solutes and particles/pathogens can therefore negatively impact the water quality, for example earlier than anticipated, if assumptions are only made based on solute transport velocities (Auckenthaler et al., 2002). While a range of factors influencing particle and solute transport behaviour have been identified so far, such as physical flow conditions, geomorphology of the system, type of used particles or particle size (Goeppert & Goldscheider, 2019; Harvey et al., 2008; Richter et al., 2022; Schiperski et al., 2016), underlying mechanisms of observed differences in flow velocities of solute tracers in contrast to particles are still not fully understood. So far, studies have mostly been performed in both epi-phreatic and phreatic conditions, but not exclusively in a fully phreatic conduit. Furthermore, detailed investigations in particular in regard to the chemical composition of the suspended sediment are lacking in previous comparative tracer tests. This, however, gives valuable information about element specific transport mechanisms. In studies that discuss the storage and remobilization of, for example heavy metals and contaminants in (cave) sediments (Gutiérrez et al., 2004; Vesper et al., 2001), there are no known input quantities of sediments and elemental loads that could be compared with measurements at the spring. The correlation between particle transport and the transport behaviour of major and trace elements is therefore not fully understood yet. This study aims at closing these knowledge gaps by performing a comparative tracer test under natural conditions, with natural sediment and the measurement of major and trace elements as well as REE.

The objectives of this study are:

1. To investigate possible differences in transport behaviour of sediment particles in contrast to solutes under natural conditions and in a fully phreatic karst conduit,
2. With a special focus on detailed transport processes and flow velocities for individual particle sizes in a large karst conduit,
3. To investigate possible differences in the transport of individual major and trace elements, REE of natural and anthropogenic origin as well as contaminants during the conduit passage in a natural karst system and

4. To improve the methodical approach of comparative tracer tests with solute tracers and sediment particles under natural conditions, by conducting the experiment in a large karst conduit with a high discharge and additionally investigating geochemical elements in the suspended sediment.

The emphasis of this study was therefore both on methodological improvements of comparative sediment tracer tests as well as a broader understanding of particle and element transport behaviour in karst systems.

2 | MATERIALS AND METHODS

2.1 | Test site

The test site is located in the Swabian Alb, Germany's largest karst landscape and karst aquifer system. The Blautopf is Germany's second largest karst spring, with a catchment area of 165 km^2. The catchment area is well defined by previous tracer tests that have been performed with solute fluorescence tracers (Selg & Schwarz, 2009). The discharge of the spring varies between 300 L/s and 32 500 L/s with an average of 2430 L/s (mean lower discharge: 616 L/s, mean highest discharge: 14 500 L/s [LfU, 2006]). The aquifer is located in Upper Jurassic limestone and marl series, with a total thickness of 400 m (Bartenbach & Ufrecht, 2009; Lauber et al., 2014). The Bluecave system is currently 16.2 km long and still under exploration. Due to diving expeditions, the 1250 m long conduit from the spring to the first cave lake (Mörikedom), that is used for the tracer test, is known and mapped in great detail (Figure 1). The conduit varies in width, in the range of several metres, and fluctuates between 468 m and 512 m above sea level. The conduit is completely water filled (phreatic) except for two small air-filled cave parts along the conduit (Ufrecht et al., 2016). Discharge measurements are performed continuously and are available upon request from the Baden Wurttemberg state environmental agency (LUBW) in 15-min intervals, the precision of the measurements is within 9% deviation from the mean value.

2.2 | Injection of conservative tracers and sediment

For the investigation of sediment transport behaviour, natural sediments from the Bluecave (Blauhöhle) were used; for particle size distribution, please refer to Figure 2. In total, 60.2 kg of cave sediment (water content 26.6%) was distributed in four tubs and 20 L of water was added to each tub (measured with buckets with a 10 L mark), further details on the sediment composition, please refer to Table 2 and Table S1. All tubs were thoroughly mixed with an electric mixer before injection. As conservative tracers, 80 g of Uranine (Fluotechnik, Les Taillades, France) and 200 g of Sulforhodamine G (Colorey, Lozanne, France) were injected.

The experiment was conducted from 15 January to 18 January 2022. All tracers were injected directly as Dirac input at a position where the cave stream forms a lake. The sediment suspensions were all injected within a timeframe of 2 min. Potential adsorption processes or measurement uncertainties, due to a high turbidity

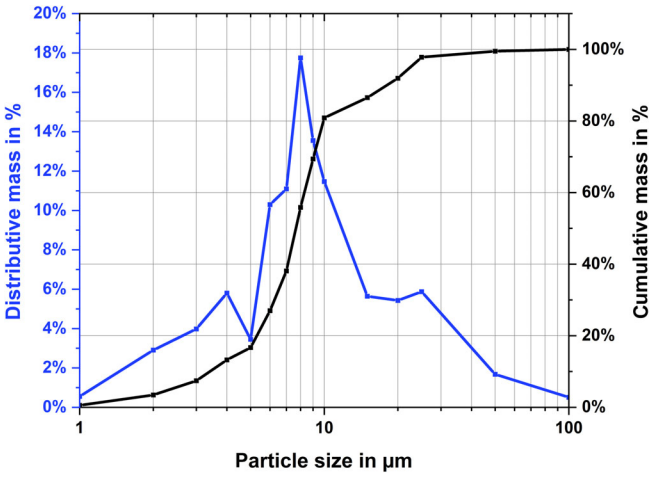

FIGURE 2 Distributive and cumulative particle size distribution by mass of the cave sediment. Masses were calculated from particle numbers with a mean particle diameter and the assumption of a spherical particle.

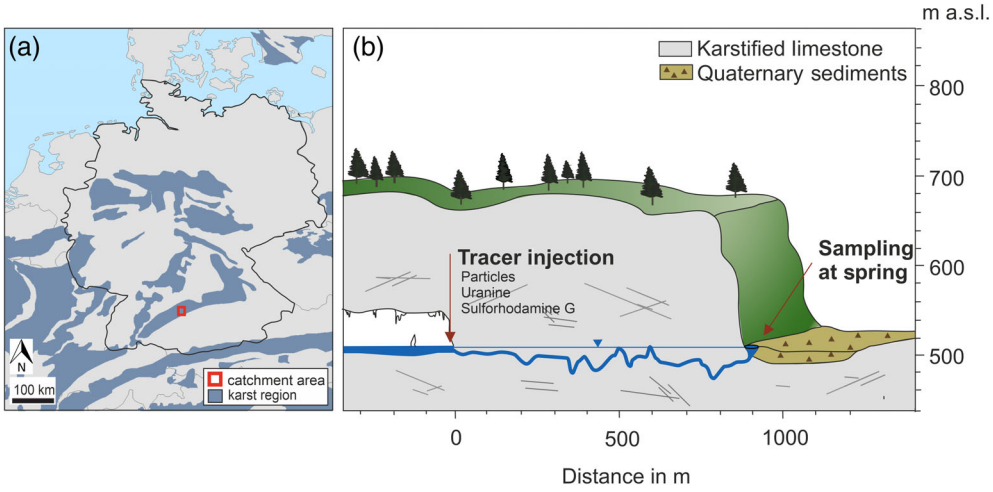

FIGURE 1 Outline of Germany with location of the catchment area of Blautopf in Southern Germany (a), modified after Chen et al. (2017). Sketch (b) of the investigated conduit, with the injection point at the beginning of the phreatic conduit and sampling point at the spring, modified after Ufrecht et al. (2016).

originating from the sediment, were avoided by injecting solute tracers 1 h after the sediment.

During the experiment, hydrological conditions were relatively constant with a slight decrease from 2010L/sto 1800 L/s, with a mean discharge of 1864 L/s (precision of discharge measurements is ±170 L/s) and no precipitation; thus, an interpretation of data due to variable discharge can be excluded.

2.3 | Sampling at the spring

The sampling of both sediment and conservative tracers took place at the spring. Due to local conditions and special requirements of the measurement instruments in regard of protection against cold, a bypass was installed (Figure S1 in SI). A pump (Geo-Inline Plus, 12 V, max. 19 L/min, Comet) was installed before the 11.8 m long bypass consisting of a lightproof mantled polyethylene tube (diameter ½", Rehau Industries, Rehau, Germany) eligible for drinking water supply (according to the German DVGW W270/KTW A). The material was chosen to avoid algae growth and limit biofilm formation. The flow rate in the bypass was regularly monitored to ensure constant flow conditions.

2.4 | Conservative tracers

Online measurements of Uranine were performed with an online field fluorimeter GGUN-FL 30 (Albillia) at an interval of 10 s. For comparison, water samples were collected with an automated sampler (Teledyne ISCO) in intervals of 20 min–4 h. All water samples were stored in 50 mL brown glass bottles in the dark at a temperature below 4°C before analysis with a LS55 fluorescence spectrometer (Perkin Elmer Inc.) in the laboratory. Both fluorimeters, GGUN-FL 30 and LS55, were calibrated with the respective tracers and water from the spring. The conservative tracers Uranine and Sulforhodamine G are both harmless for the environment (Behrens et al., 2001) and have a low detection limit of 0.005 µg/L (Uranine) and 0.05 µg/L (Sulforhodamine G) in water from Blautopf, determined by a calibration curve with the described analysis method (Goldscheider et al., 2008).

2.5 | Sediment analysis and particle size distribution

The particle size distribution (PSD) of the injected sediment suspension was analysed by dilution of 1 mL of sediment suspension in bi-distilled water, which was then measured 10 times with a particle counter (PCSS fluid lite, Klotz GmbH) in the laboratory (relative standard deviation 6%). This procedure was repeated three times to account for possible inhomogeneity in the sample (relative standard deviation 0.8% between the three subsamples). The size classes measured with the particle counter include also particles that are up to 0.9 µm larger than the respective size class, for example the size class of 1 µm include particles up to 1.9 µm. The sediment suspension contained a total number of 9.3×10^{13} particles; for a particle size distribution by mass please refer to Figure 2. Particles masses were determined based on particle numbers by assuming spherical particle diameters.

For determining particle numbers in the spring water in a size range of 1–100 µm, a mobile particle counter (PCSS fluid lite, Klotz GmbH) was installed after the bypass. The measurement interval was set to 2 min with a rinsing volume of 40 mL and a measurement volume of 10 mL for each sample. Background measurements of particle numbers at the spring were taken for 24 h prior to sediment injection and showed variabilities for particle sizes of 1–10 µm between 2.5% and 15%, whereas particle numbers decreased with increasing diameter and thus showed a generally higher variation. Background values were subtracted prior to calculation of particle recovery and modelling, which is a common practice for evaluation of tracer breakthrough curves with background (Leibundgut et al., 2009).

2.6 | Data analysis – tracer

The relative mass recoveries of solute tracers and particle recoveries were calculated with the following formula:

$$R = \frac{1}{M}\int_{t=0}^{t_{end}} (QC)\mathrm{d}t \quad (1)$$

where R is the mass- or particle recovery, M is the injected tracer quantity (solute mass or particle number), Q is the discharge and C is the tracer concentration (mass/volume or particles/volume) at time t, whereas t_0 is the time of injection and t_{end} describes the end of measurements (Käss, 2004). A time step of $t/2$ on each side of each time step was used for calculations. The formula has also been applied on sediment particles in previous studies (Goeppert & Goldscheider, 2008; Richter et al., 2022).

Basic transport parameters (peak transit time, mass- or particle recovery, maximum tracer concentration, dominating or peak flow velocity [v_{dom}]) were directly obtained from the breakthrough curves of conservative tracers and each individual particle size. All breakthrough curves were further modelled with the CXTFIT code (Toride et al., 1999) in the software STANMOD (version 2.1) (Simunek et al., 1999) using an advection-dispersion model (ADM). Mean flow velocity, dispersion and mass were fitted to data. Breakthrough curves could be sufficiently modelled with an ADM model, which contains fewer fit parameters than a 2RNE model (two-region non-equilibrium model) and therefore does not provide any ambiguous results. For a better comparison Sulforhodamine G, Uranine and all particle sizes were modelled with 2RNE nevertheless, whereas additionally the partition coefficient (β) and the mass transfer coefficient (ω) were fitted (Table S4 in SI).

2.7 | Sediment samples on filters

Water samples were manually taken every 1–4 h and directly vacuum filtered (MZ 2, Vacuubrand) on site over a 25 mm diameter cellulose acetate filter with a pore size of 0.45 µm (Sartorius) for geochemical analysis. The filtered volume was chosen to be as high as possible

within a reasonable filtration time, to assure the highest possible particle load on the filter. A filter volume between 990 mL and 2500 mL could be achieved depending on particle load. All filtration equipment was rinsed with ultrapure water prior to each sample, to avoid cross contamination between the samples. To monitor blank values throughout the sampling and analysis procedure (process blank values), 2000 mL of bi-distilled water was filtered under the same conditions as the samples in regular intervals (four blank samples in total) and treated according to the samples.

After being stored and transported in individual plastic filter boxes, sediment-loaded filters were dried at room temperature for at least 24 h and then completely digested in Teflon vials using sub-boiled HNO_3 (65%), $HClO_4$ (65%, normatom) and HF (40%, suprapure). The samples were evaporated to near dryness. Afterwards, HNO_3 (65%) was repeatedly added and evaporated to clean the digest. Finally, the samples were dissolved in 10 mL HNO_3 (1%). For quality control, blank filters and certified standards (GXR-2 and SL-1) were digested accordingly. Subsequently, the digested sediment samples, blank filters and reference standards were measured with inductively coupled plasma mass spectrometry (ICP-MS) (ICP-MS 7800, Agilent Technologies). Internal standards were used during ICP-MS measurements and a drift control was performed with a 5 µg/L internal standard for major ions and trace elements, which was used throughout the analysis. Major cations (Ca and Mg), trace elements (Li, Be, Al, V, Mn, Fe, Co, Ni, Ga, As and Rb) and REE (La, Ce, Pr, Nd, Sm, Eu, Gd, Tb, Ho, Er, Tm, Yb, Lu and Th) were measured. A list with process blank values and internal calibration standards for ICP-MS measurements can be found in (Table S2 in SI).

For evaluation of geochemical data, blank values from the test site were checked for normal distribution (Shapiro Wilk test), then outliers were determined by Grubbs test ($p = 0.05$) (Origin Lab 2021). All measurement results for sediment samples were divided by the filtered water volume to obtain a value of microgram of each element in the sediment fraction in 1 L of filtered water. Process blank values from the test site were then subtracted; these blank values included filtering of a comparable volume of bi-distilled water under field conditions, digestion and measurements with ICP-MS.

Volume corrected measurement results for B, Ti, Cu, Zn, Nb, Mo, Ag, Cd, Cs, Ta, W, Pb and Bi were below the threshold of mean process blank values plus three times standard deviation of process blank values; thus, these elements were excluded from further evaluation.

REE data were normalized to PAAS (Post Archean Shales) standard, an often-used standard for the upper continental crust (McLennan, 2001). For calculation of Ce and Gd anomalies, an interpolation of expected PAAS normalized concentrations (indicated by *) of neighbouring elements is usually used:

For calculation of Ce anomaly, the following formula was used:

$$Ce_{PAAS}/Ce_{PAAS}* = \frac{2 \times Ce_{PAAS}}{La_{PAAS} + Pr_{PAAS}} \quad (2)$$

For sediment samples the following formula was used for the calculation of Gd anomalies:

$$Gd_{PAAS}/Gd_{PAAS}* = \frac{2 \times Gd_{PAAS}}{Eu_{PAAS} + Tb_{PAAS}} \quad (3)$$

The same calculations were used for a normalization of REE data to the input values of the sediment suspension, to investigate for possible changes of anomalies during the experiment.

Grinded and dried (48 h at 60°C) samples of cave sediment from slightly different positions at the cave lake (sample 1–3) were measured for mineralogical components with X-ray diffraction (D8 Discover) and X-ray fluorescence (S4 Explorer, Bruker AXS). Results of quality control measurements of the reference standards for X-ray fluorescence are found in Table S3.

For the determination of total organic carbon, samples were dried as well (48 h at 60°C), grinded and treated with 2 M HCl (suprapure, Carl Roth) until all carbonate volatilized, then measured with a TOC vario cube (elementar).

3 | RESULTS

3.1 | General transport parameters of conservative tracers and sediment particles

All breakthrough curves have a similar shape and exhibit a single peak. The arrival times (Figure 3 and Table 1) differ significantly between particle tracers (sediment) with a mean flow velocity of 116.5–118.3 m/h, depending on particles size, and solute tracers with a mean flow velocity of 107.6 m/h (Uranine and Sulforhodamine G). The dispersion for solute tracers is slightly lower with 1552–1556 m^2/h in contrast to particles with a dispersion of 1695–1764 m^2/h. Dispersivity is similar both for particle tracers as well as solute tracers. All particles size classes show a comparable transport behaviour without significant differences. A significant difference between the particles sizes in regard of flow velocities and dispersion

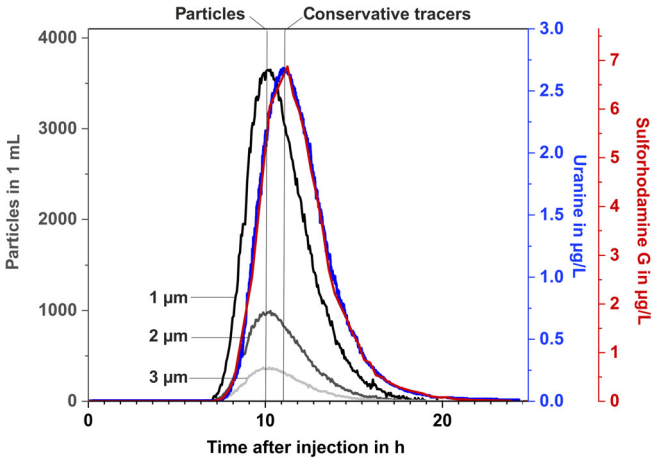

FIGURE 3 Tracer breakthrough curves for Uranine (blue), Sulforhodamine G (red), 1 µm, 2 µm and 3 µm particles (grey) with measured concentrations. Vertical bars indicate net breakthrough time of particle peaks (left) and conservative tracers (right).

TABLE 1 Transport parameters for solute tracers Uranine and Sulforhodamine G (Sulfo G) and particles, including fitted ADM parameters for the travel distance of 1250 m.

Parameter	Tracer (input)	Mass/particle recovery	Max. tracer conc.	Peak time	v_{dom}	v_{mean}[a]	Dispersion[a]	Dispersivity	
Unit	g or number of particles	%	µg/L or particles/mL	h	m/h	m/h	m^2/h	m	R^2[1]
Uranine	80	96	2.67	11.00	113	107.6 ± 0.1	1552 ± 7	14.4	0.994
Sulfo G	200	101	7.19	11.25[c]	111	107.6 ± 0.4	1560 ± 74	14.5	0.992
Total particles	9.3×10^{13}	107[b]	3650	10.17	123	116.5 ± 0.1	1735 ± 28	14.3	0.991
1 µm	3.9×10^{13}	120[b]	1709	10.05	124	116.5 ± 0.1	1735 ± 28	14.3	0.991
2 µm	2.5×10^{13}	105[b]	983	10.17	123	116.5 ± 0.1	1742 ± 29	14.4	0.991
3 µm	1.0×10^{13}	97	370	10.23	122	116.7 ± 0.1	1705 ± 30	14.0	0.990
4 µm	6.3×10^{12}	92	221	10.05	124	116.8 ± 0.2	1728 ± 33	14.2	0.988
5 µm	1.9×10^{12}	92	65	10.11	124	116.6 ± 0.2	1720 ± 41	14.2	0.982
6 µm	3.3×10^{12}	89	109	10.29	122	117.0 ± 0.2	1729 ± 37	14.2	0.985
7 µm	2.3×10^{12}	89	74	10.17	123	116.7 ± 0.2	1764 ± 40	14.5	0.983
8 µm	2.4×10^{12}	85	76	9.88	127	117.6 ± 0.2	1749 ± 41	14.3	0.982
9 µm	1.3×10^{12}	82	42	10.05	124	118.2 ± 0.2	1695 ± 45	13.8	0.977
10 µm	8.0×10^{11}	100	31	10.41	120	118.3 ± 0.3	1718 ± 52	13.9	0.970
15 µm	1.2×10^{11}	155[b]	8	9.99	125	118.6 ± 0.5	1713 ± 83	13.9	0.924

[1]R^2 for particle numbers migth be slightly overestimated due to subtraction of particle baseline.
[a]CXTFIT (ADM) model.
[b]Recoveries above 100% likely reflect uncertainties in quantification of discharge (Sulforhodamine G) and input quantity of particles.
[c]Peak time based on water samples.

could not be observed in contrast to other studies (Goeppert & Goldscheider, 2019). Breakthrough curves of Sulforhodamine G were not measured online but modelled based on water samples, which may slightly impact fitted transport parameters (different length of integration intervals of concentration) in comparison to Uranine. However, both solute tracers are considered conservative, yielded similar mass recoveries, were injected simultaneously and modelled breakthrough curves were very similar, therefore data were interpreted for travel times accordingly.

Measured tracer breakthrough curves for Uranine, Sulforhodamine G and total particles numbers (1–15 µm) are shown in Figure 3. Despite a slight tailing, all breakthrough curves could be sufficiently well modelled with the ADM (Figure 4 and Table 1) with $R^2 = 0.970$ to $R^2 = 0.993$. Whereas R^2 for particle numbers might be slightly overestimated because of zero values due to subtraction of the particle baseline.

Mass recoveries for solute tracers were 96% for Uranine and 101% for Sulforhodamine G (Figure 4). The mass recovery for both conservative tracers might result from slight measurement uncertainties, as a mass recovery over 100% is not realistic (Benischke, 2021). Adsorption to surrounding rocks or sediments were negligible as mass recovery for both tracers was very high.

Particle recoveries for individual particle size classes ranged between 82% (for 9 µm particles) and 120% (for 1 µm particles), see Table 1. A particle recovery above 100% is likely due to uncertainties in the quantification of particle numbers in the injected sediment suspension. Particles with a diameter below 1 µm could not be quantified with the particle counter and thus their transport behaviour was not in the scope of this study. Particles larger than 15 µm were not considered in the particle recovery as only very few particles arrived at the spring as larger particles are subject to increased sedimentation (Atteia & Kozel, 1997), a similar size distribution pattern with very few large particles >10 µm was also observed in other karst springs (Pronk et al., 2007; Schiperski et al., 2015).

Breakthrough curves for all particle sizes were modelled with ADM as well (Figure S2). Additionally, Uranine, SulforhodamineG and all particle sizes were modelled with the 2RNE (Figure S3 and Table S4).

3.2 | Geochemical composition of transported particles

Results from geochemical analysis go in line with the observed particle numbers during the particle peak. All elements that were measured in the sediment show a significant increase in concentrations at the time of the particle peak and return to previous levels thereafter. For a better comparison, measurement results of the elements were normalized and plotted in a heat map, whereby measurement values are normalized to c/c_{max}, respectively, the highest measured value for each element is indicated by 1 (dark purple) (Figure 5). High concentrations of elements in the sediment samples can therefore be directly

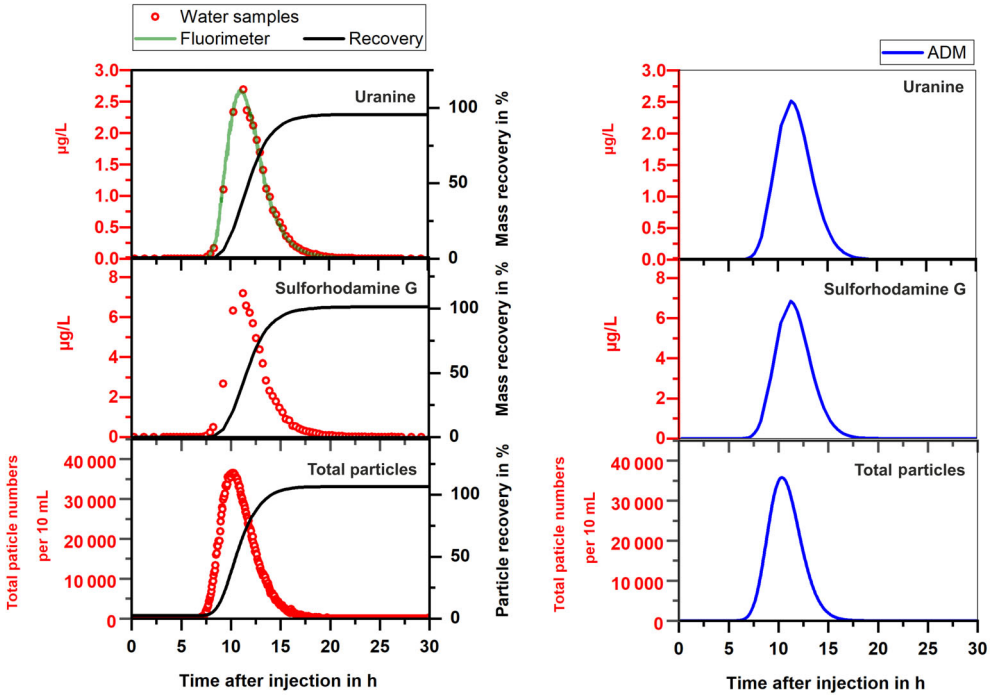

FIGURE 4 Breakthrough curves for Uranine, Sulforhodamine G and total particle numbers. Results from water samples (red dots), field fluorimeter (green) and ADM models (blue) are given in µg/L and particles in 10 mL, respectively, recovery (black) is given in percentage.

linked to the cave sediment that was artificially suspended and transported to the spring during this experiment. To allow a rough assessment of the increase in concentrations for each element in the sediment samples, bars on the right side of Figure 5 indicate the range of measured values for each element. The increase of concentrations from baseline to peak, given in µg per filtered litre of water, ranged from 3.9-fold to 16-fold.

A Spearman rank correlation was performed on measurements of geochemical elements after testing for normal distribution (Shapiro Wilk test). A correlation was considered significant with $p \leq 0.05$ and shows a significant ($p \leq 0.05$) positive correlation ($\rho > 0.7$) between all major and trace elements and REE in sediment samples, except Tl and Na, V and Mn as well as Tb and Na (Table S5 in SI). All REE in the sediment show a similar behaviour, except Dy which shows several outliers that are not relatable to any other elements. Additionally, a principal component analysis (PCA) was performed and exhibited two major components with PC1: 90.02% and PC2: 3.19% (Table S6 and Figure S4 in SI).

The overall REE (sum REE) values in sediment samples more than tripled (from 0.03 ng/L to 3.7 ng/L) during the particle peak and returned to pre-peak conditions at the same time than particle concentrations.

PAAS normalized concentrations for REE in cave sediment exhibited similar Ce and Gd anomalies as in sediment samples measured at the spring, with $Ce/Ce^* = 0.83$ and $Gd/Gd^* = 1.50$. Anomalies for sediment samples measured at the spring did not change in the course of the experiment when normalized to input quantities for Ce ($Ce/Ce^* = 0.96 \pm 0.02$) and Gd ($Gd/Gd^* = 1.01 \pm 0.04$).

Major components measured by X-ray fluorescence of the injected sediment were by percent of weight: SiO_2 (63%–68%), Al_2O_3 (15%–16%), CaO (5%–6%) and $Fe_2O_{3\ (total)}$ (5%–6%) (Table 2). The crystalline fraction of the sediment comprised mainly of quartz (>50%), calcite (approx. 10%), feldspar (approx. 15%) and mica (approx. 15%). The content of total organic carbon was 1.13%.

Sediment samples that were filtered at the spring contained moderately high amounts of Al (34.9 µg/L), Ca (21.0 µg/L), Fe (20.2 µg/L), Mg (3.11 µg/L), K (5.98 µg/L), Na (2.11 µg/L) and Mn (0.62 µg/L) during the particle peak. Mass of the respective chemical element of the suspended solids calculated in 1 L of water.

4 | DISCUSSION

4.1 | General transport parameters of conservative and sediment tracers

A similar behaviour of higher flow velocities of particles in comparison to solute tracers and thus the overall bulk velocity of water, was already observed by previous field studies (Auckenthaler et al., 2002; Goeppert & Goldscheider, 2008; Richter et al., 2022; Schiperski et al., 2016) and laboratory experiments (Ahfir et al., 2007; Toran & Palumbo, 1992). One likely explanation for higher flow velocities is a pronounced transport of particles in the main flow path and thus in the centre of larger conduits. Solute tracers, in contrast, tend to diffuse also into the low flow zone, including, for example, smaller fissures, conduit sediments and annex-to-drain zones, resulting in an overall lower mean transport velocity in contrast to particles (Goeppert & Goldscheider, 2019; Richter et al., 2022). A higher flow velocity of particles in the centre of conduits is often accompanied by a lower dispersion in contrast to solute tracers, which could also be

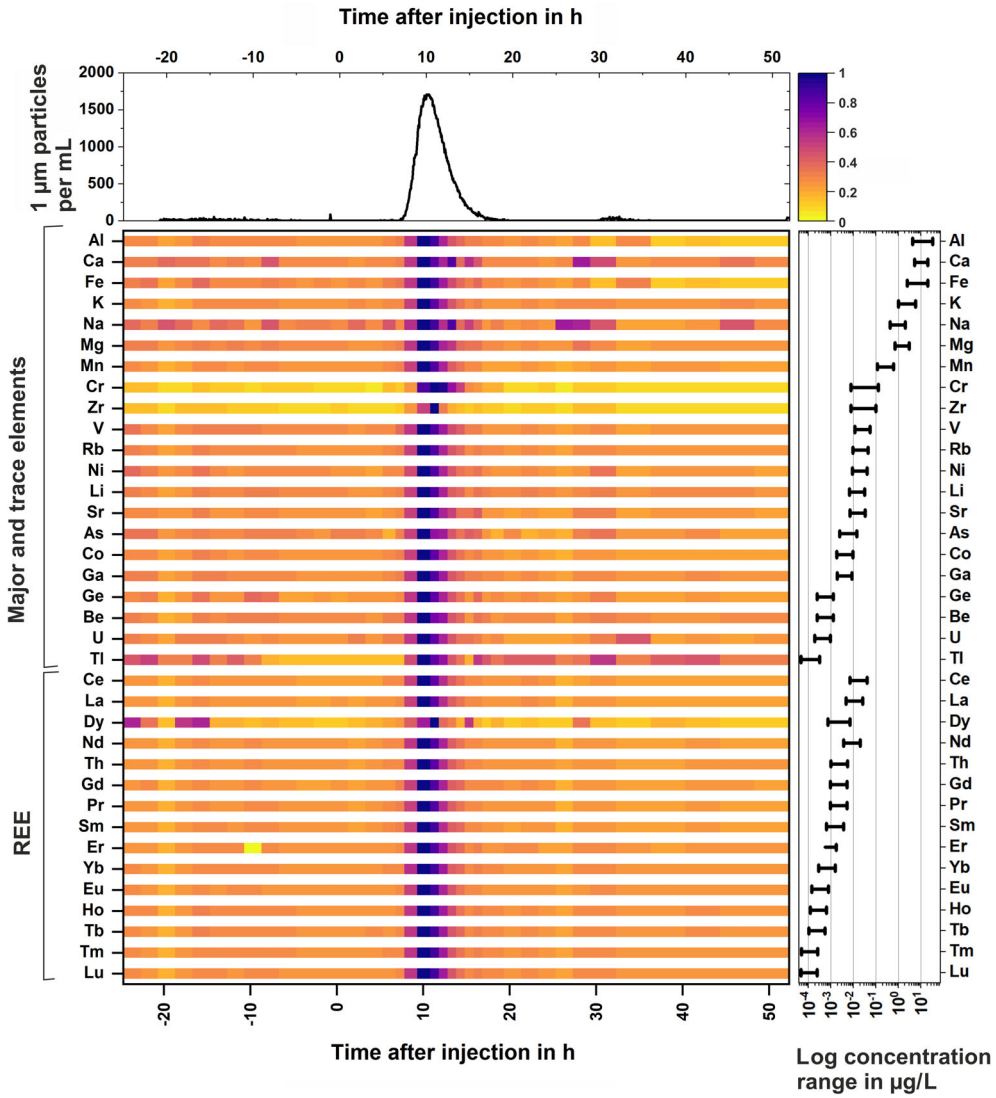

FIGURE 5 Normalized values for major and trace elements as well as REE for sediment samples. Each element was normalized to the individual maximal measurement value (c/c_{max}). Dark colours (purple) indicate highest values, whereas lighter colours (yellow) indicate the proportion of the measured concentration in contrast to the highest value. Total particle numbers are given for comparison. Concentration range of blank-corrected measurements for each element in µg/L are indicated on the logarithmic scale on the right.

TABLE 2 Geochemical analysis of cave sediment samples measured with X-ray fluorescence given in percentage of weight.

	% by weight											
Sample	Na_2O	MgO	Al_2O_3	SiO_2	P_2O_5	K_2O	CaO	TiO_2	MnO	Fe_2O_3—total	Ignition loss	SUM (%)
Sample 1	0.56	1.3	16.4	62.3	0.56	1.7	6.1	0.92	0.24	5.8	11.7	107.6
Sample 2	0.58	1.3	15.1	63.4	0.56	1.6	6.7	0.91	0.24	5.7	11.5	107.6
Sample 3	0.66	1.1	14.5	68.3	0.39	1.7	5.0	0.93	0.25	5.3	9.6	107.7

shown mathematically for fractures and uniform tubes (James & Chrysikopoulos, 2003). However, this is not always the only effect present and particles can as well exhibit both a higher flow velocity and a slightly higher dispersion than solute tracers (Goeppert & Goldscheider, 2008; Toran & Palumbo, 1992), which goes in line with the slightly higher dispersion of particles during the described experiment, whereas dispersivity is similar both for solute tracers and particles. As the ADM is a simplified approach for comparison of transport parameters that has been used in previous literature (Field & Li, 2011), differences in dispersion can only serve as a hint, but further experiments would be required to investigate these processes more in depth. In other studies, higher flow velocities of particles in contrast to solutes are also explained as pore exclusion processes, whereas particles are too large to enter smaller pores and therefore transported faster (Schiperski et al., 2016), however these processes are likely more relevant for the vadose zone and are only of minor relevance for this tracer test in a fully phreatic conduit. A significant difference between the particle sizes in regard of transport velocities and dispersion could not be observed in contrast to other studies (Goeppert & Goldscheider, 2019; Richter et al., 2022), which might be

a result of a larger conduit cross section of several meters with a large preferential flow path for all particle sizes. The transport behaviour for particles smaller than 1 μm, which may differ from larger particles, is beyond the scope of this study.

Differences in transport velocities can further be impacted by flow conditions, whereby high and more turbulent flow conditions seem to favour more similar transport velocities of particles and solutes and vice versa (Goeppert & Goldscheider, 2011; Richter et al., 2022). As flow conditions during the experiment were constant, an influence of changing hydrological conditions on transport velocities can be ruled out. The average discharge of 1864 L/s during the experiment was slightly below the average annual discharge of 2330 L/s (Selg & Schwarz, 2009). Faster flow velocities of particles opposed to solutes are therefore to be expected, as differences between those two phases are particularly pronounced at low flow conditions (Goeppert & Goldscheider, 2008; Richter et al., 2022).

It is supposed that the specific conditions at the injection site may have contributed to the faster transport of particles compared to solutes. Solute tracers and particles were injected from the same position within the cave system, into the cave lake above the entrance of the fully saturated conduit (Figure S5 in SI). Visual observations showed a slightly quicker entry of particles into the downward leading conduit, potentially due to gravity effects of the dense sediment suspension or small particle clusters. In comparison to the solute tracers, Uranine and Sulforhodamine G, which showed a higher lateral distribution and were longer visible in the water. However, dye tracers in general have a rather high visibility to the naked eye.

Particle recoveries decrease with increasing particle diameter, which can be attributed to an increased sedimentation of particles >5 μm (Atteia & Kozel, 1997; Goeppert & Goldscheider, 2019; Schiperski et al., 2015). Due to the natural conditions in the cave, it was further very difficult to assess correct input quantities for particle numbers and particle recoveries. Besides, large sediment amounts (60.2 kg) and suspected inhomogeneity of the sediment suspension, in particular particle clusters as well as coagulation processes of small particles, may have led to a slight underestimation of particle numbers in the lower micrometre range for the injected sediment suspension, resulting in an overestimation of the recovery rate. Particle clusters may result from sedimentation, storage in the tubs and possibly also transport of samples as well as changes in zeta potential during dilution of the sediment suspension with bi-distilled water in the laboratory (Hsu & Liu, 1998; Mingard et al., 2009), which would have increased particle recoveries in particular of small particles. Effects resulting from transport and sub-sampling of the injected sediment suspension were unfortunately inevitable due to site-specific conditions in the cave. Nevertheless, maximum care was taken from sampling to repeated measurements of the sub-samples of the injected sediment suspension. Particle recoveries are therefore interpreted with care and do not impact general transport parameters and geochemical analysis. Previous studies of comparative tracer tests yielded variable particle recoveries between 20% and 99% (Goeppert & Goldscheider, 2008, 2019; Richter et al., 2022; Schiperski et al., 2016). In this study only on large, well-known conduit was investigated without major branching, which could further contribute to a high particle recovery.

4.2 | Geochemical composition of transported particles

A sediment-associated transport could be observed for all geochemical elements that were measured in the sediment samples, both with a geogenic, for example Ca, Mg, Al, and additional anthropogenic origin, for example Gd, as described below. Even during large storm events, the major sediment composition does not differ from the base flow (Herman et al., 2008).

Besides being incorporated into, for example, silicates (Marks & Markl, 2014), dissolved REE often attach to iron (hydr)oxides and organic matter (Andersson et al., 2006; Matsunaga et al., 2014). A transport of REE with the suspended sediment was expected and could be seen (Figure 3). For the sediment samples in this study, a more positive Ce anomaly would have been expected as Ce is less soluble under oxidizing conditions (Braun et al., 1990; Brioschi et al., 2013). A positive Gd anomaly in the injected sediment, that was also found in the sediment samples measured at the spring, with $Gd/Gd^* = 1.50$, can be linked to anthropogenic inputs of Gd from, for example, magnetic resonance imaging (MRI) contrasting agents (Bau & Dulski, 1996; Brioschi et al., 2013; Knappe et al., 2005). Anthropogenic input of Gd at the study site is very likely as waste water treatment plants are located in the catchment area of the karst system. When normalized to input quantities, the anomalies for Ce and Gd remained similar over the course of the experiment, thus no fractionation of Ce and Gd occurred during the conduit passage.

In previous studies (Bau & Dulski, 1996; Brünjes & Hofmann, 2020; Knappe et al., 2005), Gd has been analysed primarily in water samples, whereas in this study, the transport of Gd was analysed in particulate form. A positive Gd anomaly was found throughout the entire experiment. This supports the assumption that dissolved Gd from anthropogenic sources may be retained in sediments and be remobilized as well in its particulate form by storm events. A similar behaviour was also observed for other anthropogenic contaminants (Vesper et al., 2001).

All geochemical elements show a strong increase in concentration in the particulate fraction upon the arrival of the particle peak, which is directly linked to the injected sediment suspension, reflecting a (simulated) transport of naturally occurring sediments. In contrast to artificial tracers, transport processes of natural sediment, respectively, natural geochemical behaviour, could be investigated in the experiment, imitating a natural turbidity event. The sediment which was suspended during the comparative tracer test originates from natural sediment deposits in the cave system. Often these sediments are remobilized during heavy rainfalls as shear flows increase (Cholet et al., 2019; Herman et al., 2008; Husic et al., 2017).

Karst systems share common chemical properties, such as circumneutral to alkaline pH, and minerals, such as calcite and often dolomite. However, major and trace element concentrations usually vary

between different systems and can even show a seasonal variability (Klimchouk, 2017; Stecko & Bendell-Young, 2000; Vesper & White, 2004). Thus, it is important to understand site-specific physical and chemical transport processes, which was done by performing the experiment with cave sediments from the Bluecave system.

5 | CONCLUSIONS

The comparative sediment tracer test in a fully phreatic conduit showed a particle transport in preferential flow paths, and thus, significantly increased flow velocities of particles in contrast to solute tracers. Both conservative tracers, Uranine and Sulforhodamine G, showed a similar transport behaviour during the experiment, therefore adsorption processes to surrounding rocks or sediments were not relevant during the conduit passage. A different transport behaviour with respect to different particle sizes could not be observed, as all particle sizes yielded comparable transport velocities.

Geochemical analysis supports a preferential sediment associated transport for all analysed major and trace elements and REE, which could be seen in a clear increase of element concentrations during the particle breakthrough curve. An anthropogenic input of Gd could be observed in anomalies when standardized to PAAS, but no further change in anomalies occurred during the conduit passage. Such a sediment-associated transport of anthropogenic Gd may apply to other anthropogenic contaminants as well.

The approach of a comparative tracer test with conservative tracers and sediment particles in a natural karst system could be successfully applied in a large karst conduit with a high discharge (>1800 L/s). Distinct breakthrough curves for both solute tracers and particles with diameters from 1 μm to 15 μm could be achieved. Measurements of geochemical elements in the suspended cave sediment provided further information on element-specific transport behaviour, which gives a hint on processes occurring during natural turbidity events for a specific karst system.

Our findings demonstrate a suitable approach to investigate turbidity-associated transport processes in karst systems by performing a comparative tracer test with particles and solutes and an additional measurement of the chemical composition of the sediment. An investigation of these transport processes can help to understand changes of the water quality in karst springs in more detail.

ACKNOWLEDGEMENTS

We thank the German Research Foundation (DFG) for funding this study as part of the IMPART project (project number: 432288610). We acknowledge support by the KIT-Publication Fund of the Karlsruhe Institute of Technology. The authors gratefully acknowledge the provision of discharge data from the State Office for the Environment, Measurements and Nature Conservation of the Federal State of Baden-Württemberg (LUBW). In particular, we express our special thanks to the speleologists of ARGE Blautopf, without whom this research would not be possible, specifically Andreas Kücha, Jens Freigang, Marco Scheuer and Matthias López Correa. We also thank the city of Blaubeuren and Mr. Schönhofer for their practical support and provision of the premises at Blautopf. We especially thank Markus Klotz for constructing a split after the bypass for adequate sampling with the particle counter. Likewise, our special thanks go to the hydrogeology and geochemistry laboratory team members at the KIT. We also thank Jiawen Zhang for providing a section of the WOKAM map and the MVM institute at KIT for lending filtration equipment. For fruitful discussions on REE data we thank Brian Berkowitz and Ishai Dror from Weizmann Institute of Science, Israel. We further give a special thanks to both the anonymous reviewers whose comments helped to significantly improve this article, in particular for all the thorough effort and constructive comments on our article from Reviewer 1. Open Access funding enabled and organized by Projekt DEAL.

DATA AVAILABILITY STATEMENT

Data are available upon reasonable request from the corresponding author.

ORCID

Yanina K. Mueller https://orcid.org/0000-0002-2850-5460
Nico Goldscheider https://orcid.org/0000-0002-8428-5001
Elisabeth Eiche https://orcid.org/0000-0002-1493-9161
Hanna Emberger https://orcid.org/0000-0001-7914-774X
Nadine Goeppert https://orcid.org/0000-0002-6646-3791

REFERENCES

Adetutu, E., Thorpe, K., Shahsavari, E., Bourne, S., Cao, X., Fard, R., Kirby, G., & Ball, A. (2012). Bacterial community survey of sediments at Naracoorte caves, Australia. *International Journal of Speleology*, *41*(2), 137–147. https://doi.org/10.5038/1827-806X.41.2.2

Ahfir, N.-D., Wang, H. Q., Benamar, A., Alem, A., Massei, N., & Dupont, J.-P. (2007). Transport and deposition of suspended particles in saturated porous media: hydrodynamic effect. *Hydrogeology Journal*, *15*(4), 659–668. https://doi.org/10.1007/s10040-006-0131-3

Aide, M., & Nakajima, T. (2020). *Rare earth elements and their minerals* (1st ed.). IntechOpen. https://doi.org/10.5772/intechopen.77602

Andersson, K., Dahlqvist, R., Turner, D., Stolpe, B., Larsson, T., Ingri, J., & Andersson, P. (2006). Colloidal rare earth elements in a boreal river: Changing sources and distributions during the spring flood. *Geochimica et Cosmochimica Acta*, *70*(13), 3261–3274. https://doi.org/10.1016/j.gca.2006.04.021

Atteia, O., & Kozel, R. (1997). Particle size distributions in waters from a karstic aquifer: From particles to colloids. *Journal of Hydrology*, *201*(1–4), 102–119. https://doi.org/10.1016/S0022-1694(97)00033-4

Auckenthaler, A., Raso, G., & Huggenberger, P. (2002). Particle transport in a karst aquifer: Natural and artificial tracer experiments with bacteria, bacteriophages and microspheres. *Water Science and Technology*, *46*(3), 131–138. https://doi.org/10.2166/wst.2002.0072

Bartenbach, M., & Ufrecht, W. (2009). Stratigraphie und Fazies des Oberjuras im Umfeld der Blaubeurer Talschlinge – Ergebnisse einer Bohrung und Untertagekartierung im Blauhöhlensystem. *Laichinger Höhlenfreund*, *44*, 89–106.

Bau, M., & Dulski, P. (1996). Anthropogenic origin of positive gadolinium anomalies in river waters. *Earth and Planetary Science Letters*, *143*(1–4), 245–255. https://doi.org/10.1016/0012-821X(96)00127-6

Behrens, H., Beims, U., Dieter, H., Dietze, G., Eikmann, T., Grummt, T., Hanisch, H., Henseling, H., Käss, W., Kerndorff, H., Leibundgut, C.,

Müller-Wegener, U., Rönnefahrt, I., Scharenberg, B., Schleyer, R., Schloz, W., & Tilkes, F. (2001). Toxicological and ecotoxicological assessment of water tracers. *Hydrogeology Journal*, *9*(3), 321–325. https://doi.org/10.1007/s100400100126

Benischke, R. (2021). Review: Advances in the methodology and application of tracing in karst aquifers. *Hydrogeology Journal*, *29*(1), 67–88. https://doi.org/10.1007/s10040-020-02278-9

Braun, J.-J., Pagel, M., Muller, J.-P., Bilong, P., Michard, A., & Guillet, B. (1990). Cerium anomalies in lateritic profiles. *Geochimica et Cosmochimica Acta*, *54*(3), 781–795. https://doi.org/10.1016/0016-7037(90)90373-S

Brioschi, L., Steinmann, M., Lucot, E., Pierret, M. C., Stille, P., Prunier, J., & Badot, P. M. (2013). Transfer of rare earth elements (REE) from natural soil to plant systems: Implications for the environmental availability of anthropogenic REE. *Plant and Soil*, *366*(1–2), 143–163. https://doi.org/10.1007/s11104-012-1407-0

Brünjes, R., & Hofmann, T. (2020). Anthropogenic gadolinium in freshwater and drinking water systems. *Water Research*, *182*, 115966. https://doi.org/10.1016/j.watres.2020.115966

Chen, Z., Auler, A. S., Bakalowicz, M., Drew, D., Griger, F., Hartmann, J., Jiang, G., Moosdorf, N., Richts, A., Stevanovic, Z., Veni, G., & Goldscheider, N. (2017). The world Karst aquifer mapping project: Concept, mapping procedure and map of Europe. *Hydrogeology Journal*, *25*(3), 771–785. https://doi.org/10.1007/s10040-016-1519-3

Cholet, C., Steinmann, M., Charlier, J.-B., & Denimal, S. (2019). Characterizing fluxes of trace metals related to dissolved and suspended matter during a storm event: Application to a karst aquifer using trace metals and rare earth elements as provenance indicators. *Hydrogeology Journal*, *27*(1), 305–319. https://doi.org/10.1007/s10040-018-1859-2

Churchman, G. J., & Velde, B. (2019). *Soil clays: Linking geology, biology, agriculture, and the environment*. CRC Press Taylor & Frances Group.

Field, M., & Li, G. (2011). Inversion for the input history of a dye tracing experiment. *Journal of Cave and Karst Studies*, *73*(1), 16–20. https://doi.org/10.4311/jcks2010es0143

Goeppert, N., & Goldscheider, N. (2008). Solute and colloid transport in karst conduits under low- and high-flow conditions. *Ground Water*, *46*(1), 61–68. https://doi.org/10.1111/j.1745-6584.2007.00373.x

Goeppert, N., & Goldscheider, N. (2011). Transport and variability of fecal bacteria in carbonate conglomerate aquifers. *Ground Water*, *49*(1), 77–84. https://doi.org/10.1111/j.1745-6584.2010.00741.x

Goeppert, N., & Goldscheider, N. (2019). Improved understanding of particle transport in karst groundwater using natural sediments as tracers. *Water Research*, *166*, 115045. https://doi.org/10.1016/j.watres.2019.115045

Goldscheider, N., & Drew, D. (2007). *Methods in Karst hydrogeology. IAH: International contributions to hydrogeology: Vol. 26* (1st ed.). Taylor & Francis.

Goldscheider, N., Hunkeler, D., & Rossi, P. (2006). Review: Microbial biocenoses in pristine aquifers and an assessment of investigative methods. *Hydrogeology Journal*, *14*(6), 926–941. https://doi.org/10.1007/s10040-005-0009-9

Goldscheider, N., Meiman, J., Pronk, M., & Smart, C. (2008). Tracer tests in karst hydrogeology and speleology. *International Journal of Speleology*, *37*(1), 27–40. https://doi.org/10.5038/1827-806x.37.1.3

Gutiérrez, M., Neill, H., & Grand, R. V. (2004). Metals in sediments of springs and cave streams as environmental indicators in karst areas. *Environmental Geology*, *46*(8), 1079–1085. https://doi.org/10.1007/s00254-004-1110-4

Gwenzi, W., Mangori, L., Danha, C., Chaukura, N., Dunjana, N., & Sanganyado, E. (2018). Sources, behaviour, and environmental and human health risks of high-technology rare earth elements as emerging contaminants. *The Science of the Total Environment*, *636*, 299–313. https://doi.org/10.1016/j.scitotenv.2018.04.235

Harvey, R. W., Metge, D. W., Shapiro, A. M., Renken, R. A., Osborn, C. L., Ryan, J. N., Cunningham, K. J., & Landkamer, L. (2008). Pathogen and chemical transport in the karst limestone of the Biscayne aquifer: 3. Use of microspheres to estimate the transport potential of Cryptosporidium parvum oocysts. *Water Resources Research*, *44*(8), W08431. https://doi.org/10.1029/2007WR006060

Herman, E. K., Toran, L., & White, W. B. (2008). Threshold events in spring discharge: Evidence from sediment and continuous water level measurement. *Journal of Hydrology*, *351*(1–2), 98–106. https://doi.org/10.1016/j.jhydrol.2007.12.001

Horowitz, A., & Elrick, K. A. (1987). The relation of stream sediment surface area, grain size and composition to trace element chemistry. *Applied Geochemistry*, *2*, 437–451. https://doi.org/10.1016/0883-2927(87)90027-8

Horowitz, A. J., Elrick, K. A., & Smith, J. J. (2008). Monitoring urban impacts on suspended sediment, trace element, and nutrient fluxes within the City of Atlanta, Georgia, USA: Program design, methodological considerations, and initial results. *Hydrological Processes*, *22*(10), 1473–1496. https://doi.org/10.1002/hyp.6699

Hsu, J.-P., & Liu, B.-T. (1998). Critical coagulation concentration of a colloidal suspension at high particle concentrations. *The Journal of Physical Chemistry B*, *102*(2), 334–337. https://doi.org/10.1021/jp971817q

Huang, B., Yuan, Z., Li, D., Zheng, M., Nie, X., & Liao, Y. (2020). Effects of soil particle size on the adsorption, distribution, and migration behaviors of heavy metal(loid)s in soil: A review. *Environmental Science. Processes & Impacts*, *22*(8), 1596–1615. https://doi.org/10.1039/d0em00189a

Husic, A., Fox, J., Agouridis, C., Currens, J., Ford, W., & Taylor, C. (2017). Sediment carbon fate in phreatic karst (part 1): Conceptual model development. *Journal of Hydrology*, *549*, 179–193. https://doi.org/10.1016/j.jhydrol.2017.03.052

James, S. C., & Chrysikopoulos, C. V. (2003). Effective velocity and effective dispersion coefficient for finite-sized particles flowing in a uniform fracture. *Journal of Colloid and Interface Science*, *263*(1), 288–295. https://doi.org/10.1016/S0021-9797(03)00254-6

Jung, A.-V., Le Cann, P., Roig, B., Thomas, O., Baurès, E., & Thomas, M.-F. (2014). Microbial contamination detection in water resources: Interest of current optical methods, trends and needs in the context of climate change. *International Journal of Environmental Research and Public Health*, *11*(4), 4292–4310. https://doi.org/10.3390/ijerph110404292

Käss, W. (2004). *Geohydrologische Markierungstechnik: Mit 43 Tabellen (2., überarb. Aufl.). Lehrbuch der Hydrogeologie: Bd. 9*. Borntraeger.

Klimchouk, A. (2017). *Hypogene Karst regions and caves of the world*. Cave and Karst Systems of the World Ser. Springer International Publishing.

Knappe, A., Möller, P., Dulski, P., & Pekdeger, A. (2005). Positive gadolinium anomaly in surface water and ground water of the urban area Berlin, Germany. *Geochemistry*, *65*(2), 167–189. https://doi.org/10.1016/j.chemer.2004.08.004

Künnemeyer, J., Terborg, L., Meermann, B., Brauckmann, C., Möller, I., Scheffer, A., & Karst, U. (2009). Speciation analysis of gadolinium chelates in hospital effluents and wastewater treatment plant sewage by a novel HILIC/ICP-MS method. *Environmental Science & Technology*, *43*(8), 2884–2890. https://doi.org/10.1021/es803278n

LaMoreaux, J. W. (2019). *Environmental geology: A volume in the Encyclopedia of sustainability science and technology* (2nd ed.). Springer US. https://doi.org/10.1007/978-1-4939-8787-0

Lauber, U., Ufrecht, W., & Goldscheider, N. (2014). Spatially resolved information on karst conduit flow from in-cave dye tracing. *Hydrology and Earth System Sciences*, *18*(2), 435–445. https://doi.org/10.5194/hess-18-435-2014

Leibundgut, C., Maloszewski, P., & Külls, C. (2009). *Tracers in hydrology* (1st ed.). Wiley-Blackwell.

LfU - Bayrisches Landesamt für Umwelt. (2006). *Deutsches Gewässerkundliches Jahrbuch: Donaugebiet*. Augsburg.

Mahler, B., Personné, J.-C., Lods, G., & Drogue, C. (2000). Transport of free and particulate-associated bacteria in karst. *Journal of Hydrology*,

238(3–4), 179–193. https://doi.org/10.1016/S0022-1694(00)00324-3

Marks, M., & Markl, G. (2014). *Minerale und gesteine: Mineralogie – petrologie – geochemie* (3. Aufl. 2015). Springer.

Matsunaga, T., Tsuduki, K., Yanase, N., Kritsananuwat, R., Hanzawa, Y., & Naganawa, H. (2014). Increase in rare earth element concentrations controlled by dissolved organic matter in river water during rainfall events in a temperate, small forested catchment. *Journal of Nuclear Science and Technology*, *52*, 1–16. https://doi.org/10.1080/00223131.2014.961989

McLennan, S. M. (2001). Relationships between the trace element composition of sedimentary rocks and upper continental crust. *Geochemistry Geophysics Geosystems*, *2*, 1021. https://doi.org/10.1029/2000GC000109.

Mingard, K., Morrell, R., Jackson, P., Lawson, S., Patel, S., & Buxton, R. (2009). *Measurement good practice guide No.111: Good practice guide for improving the consistency of particle size measurement*. National Physical Laboratory.

Möller, P., Dulski, P., Bau, M., Knappe, A., Pekdeger, A., & Sommer-von Jarmersted, C. (2000). Anthropogenic gadolinium as a conservative tracer in hydrology. *Journal of Geochemical Exploration*, *69–70*, 409–414. https://doi.org/10.1016/S0375-6742(00)00083-2

O'Connor, A. E., Luek, J. L., McIntosh, H., & Beck, A. J. (2015). Geochemistry of redox-sensitive trace elements in a shallow subterranean estuary. *Marine Chemistry*, *172*, 70–81. https://doi.org/10.1016/j.marchem.2015.03.001

Pronk, M., Goldscheider, N., & Zopfi, J. (2006). Dynamics and interaction of organic carbon, turbidity and bacteria in a karst aquifer system. *Hydrogeology Journal*, *14*(4), 473–484. https://doi.org/10.1007/s10040-005-0454-5

Pronk, M., Goldscheider, N., & Zopfi, J. (2007). Particle-size distribution as indicator for fecal bacteria contamination of drinking water from karst springs. *Environmental Science & Technology*, *41*(24), 8400–8405. https://doi.org/10.1021/es071976f

Richter, D., Goeppert, N., & Goldscheider, N. (2022). New insights into particle transport in karst conduits using comparative tracer tests with natural sediments and solutes during low-flow and high-flow conditions. *Hydrological Processes*, *36*(1), e14472. https://doi.org/10.1002/hyp.14472

Schiperski, F., Zirlewagen, J., Hillebrand, O., Licha, T., & Scheytt, T. (2015). Preliminary results on the dynamics of particles and their size distribution at a karst spring during a snowmelt event. *Journal of Hydrology*, *524*, 326–332. https://doi.org/10.1016/j.jhydrol.2015.02.035

Schiperski, F., Zirlewagen, J., & Scheytt, T. (2016). Transport and attenuation of particles of different density and surface charge: A Karst aquifer Field study. *Environmental Science & Technology*, *50*(15), 8028–8035. https://doi.org/10.1021/acs.est.6b00335

Selg, M., & Schwarz, K. (2009). Am Puls der schönen Lau – zur Hydrogeologie des Blautopf-Einzugsgebietes. *Laichinger Höhlenfreund*, *44*, 45–72.

Simunek, J., van Genuchten, M. T., Sejna, M., Toride, N., & Leij, F. J. (1999). *The STANMOD computer software for evaluating solute transport in porous media using analytical solutions of convection-dispersion equation: Versions 1.0 and 2.0 (IGWMC-TPS 71)*. U.S. Salinity Laboratory, Agricultural Research Service.

Sinreich, M., Flynn, R., & Zopfi, J. (2009). Use of particulate surrogates for assessing microbial mobility in subsurface ecosystems. *Hydrogeology Journal*, *17*(1), 49–59. https://doi.org/10.1007/s10040-008-0362-6

Stecko, J., & Bendell-Young, L. I. (2000). Contrasting the geochemistry of suspended particulate matter and deposited sediments within an estuary. *Applied Geochemistry*, *15*(6), 753–775. https://doi.org/10.1016/S0883-2927(99)00090-6

Stevanović, Z. (2019). Karst waters in potable water supply: A global scale overview. *Environmental Earth Sciences*, *78*(23), 1–12. https://doi.org/10.1007/s12665-019-8670-9

Toran, L., & Palumbo, A. V. (1992). Colloid transport through fractured and unfractured laboratory sand columns. *Journal of Contaminant Hydrology*, *9*(3), 289–303. https://doi.org/10.1016/0169-7722(92)90009-4

Toride, N., Leij, F. J., & von Genuchten, M. T. (1999). *The CXTFIT code for estimating transport parameters from laboratory or Field tracer experiments: Version 2.1 (2.1st ed.). Research report: Vol. 137*. U. S. Salinity Laboratory.

Ufrecht, W., Bohnert, J., & Jantschke, H. (2016). Ein konzeptionelles Modell der Verkarstungsgeschichte für das Einzugsgebiet des Blautopfs (mittlere Schwäbische Alb). *Laichinger Höhlenfreund*, *51*(21), 3–44.

Vesper, D. J., Loop, C. M., & White, W. B. (2001). Contaminant transport in karst aquifers. *Theoretical and Applied Karstology*, *13*, 63–73.

Vesper, D. J., & White, W. B. (2004). Spring and conduit sediments as storage reservoirs for heavy metals in karst aquifers. *Environmental Geology*, *45*(4), 481–493. https://doi.org/10.1007/s00254-003-0899-6

Vuilleumier, C., Jeannin, P.-Y., Hessenauer, M., & Perrochet, P. (2021). Hydraulics and turbidity generation in the milandre cave (Switzerland). *Water Resources Research*, *57*(8), 1–18. https://doi.org/10.1029/2020WR029550

Zhu, H.-Z., Zhang, Z.-F., Zhou, N., Jiang, C.-Y., Wang, B.-J., Cai, L., & Liu, S.-J. (2019). Diversity, distribution and co-occurrence patterns of bacterial communities in a Karst cave system. *Frontiers in Microbiology*, *10*, 1726. https://doi.org/10.3389/fmicb.2019.01726

SUPPORTING INFORMATION

Additional supporting information can be found online in the Supporting Information section at the end of this article.

How to cite this article: Mueller, Y. K., Goldscheider, N., Eiche, E., Emberger, H., & Goeppert, N. (2023). From cave to spring: Understanding transport of suspended sediment particles in a fully phreatic karst conduit using particle analysis and geochemical methods. *Hydrological Processes*, *37*(10), e14979. https://doi.org/10.1002/hyp.14979